Optical susceptibilities of $Na_3La_9O_3(BO_3)_8$, ternary oxyborate nonlinear single crystal: theory and experiment

2008 J. Phys.: Condens. Matter 20 145209

(http://iopscience.iop.org/0953-8984/20/14/145209)

J. Phys.: Condens. Matter **20** (2008) 145209 (7pp) doi:10.1088/0953-8984/20/14/145209

Optical susceptibilities of $Na_3La_9O_3(BO_3)_8$, ternary oxyborate nonlinear single crystal: theory and experiment

Ali Hussain Reshak[1,2], **S Auluck**[3] **and I V Kityk**[4,5]

[1] Institute of Physical Biology, South Bohemia University, Nove Hrady 37333, Czech Republic
[2] Institute of System Biology and Ecology-Academy of Sciences, Nove Hrady 37333, Czech Republic
[3] Physics Department, Indian Institute of Technology, Kanpur (UP) 208016, India
[4] Institue of Physics, J Dlugosz University Czestochowa, Al. Armii Krajowej 13/15, Czestochowa, Poland
[5] Department of Chemistry, Silesian University of Technology, ul. Marcina Strzody 9, PL-44100 Gliwice, Poland

E-mail: maalidph@yahoo.co.uk (A H Reshak)

Received 18 December 2007, in final form 25 February 2008
Published 18 March 2008
Online at stacks.iop.org/JPhysCM/20/145209

Abstract

Experimental and theoretical simulations of linear and nonlinear optical susceptibilities of the novel $Na_3La_9O_3(BO_3)_8$, a ternary oxyborate nonlinear single crystal, are reported here. The calculations were based on one of the most accurate methods for the computation of the linear and nonlinear optical susceptibilities of solids within density functional theory. Our calculations show that the edges of optical absorption for $\varepsilon_2^{\perp}(\omega)$ and $\varepsilon_2^{\parallel}(\omega)$ are located at 5.2 eV, in good agreement with our measurements. The anisotropy is in good agreement with the theoretical data. The same is true for the birefringence. We found that our calculated and measured refractive indices are in good agreement with those obtained by previous measurements. The imaginary and real parts of the second order second harmonic generation (SHG) susceptibility $\chi^{(2)}_{222}(\omega)$ and $\chi^{(2)}_{112}(\omega)$ were evaluated. Our calculation shows that $\chi^{(2)}_{112}(\omega)$ is the dominant component, which shows the largest total Re $\chi^{(2)}_{ijk}(0)$ value (2.3 pm V^{-1}) compared to $\chi^{(2)}_{222}(\omega)$. This value shows very good agreement with experimental data (2.0 pm V^{-1}) obtained by previous measurements and our measurements. One specific feature of the investigated crystals consists in substantial anisotropy of their properties, which plays a crucial role in the observed experimental dependences.

These crystals possess very highly nonlinear optical properties. The coefficient of the SHG is about three to five times larger than that of KH_2PO_4 (KDP).

(Some figures in this article are in colour only in the electronic version)

1. Introduction

$Na_3La_9O_3(BO_3)_8$ (NLBO), ternary oxyborate nonlinear single crystals have been extensively investigated because of their potential applications in nonlinear optics (NLO) and laser engineering. It has excellent properties such as short growth period, large effective nonlinear coefficient, high damage threshold, and good mechanical properties. $Na_3La_9O_3(BO_3)_8$ is optically transparent from 270 to 2100 nm, free from moisture and chemically very stable [1]. This crystal was

obtained by Wu *et al* [2]. Gravereau *et al* [1] reported the preparation of the single crystal and solved its crystal structure. The unique structural characteristics of the boron–oxygen groups in a series of these compounds determine their enhanced ultra-violet transparency, very good nonlinearity and relatively high resistance against laser-induced damage [1]. The diversity and versatility of borate structures due to the flexibility of boron to adopt either trigonal or tetrahedral oxygen coordination are probably the cause of the great variety of properties in borates. Thus, in a series of these compounds, the structural characteristics of the boron–oxygen groups determine their enhanced ultra-violet transparency, which, combined with a high polarizability and resistance against radiation-induced damage, implies that many borates are attractive candidates for laser hosts and nonlinear optical materials with harmonic generation applications [3–10]. Zhang *et al* [8] reported that the optical second harmonic generation (SHG) measurements of laser radiation showed that NLBO crystal exhibits an optical SHG effect which is about three to five times larger than that of KDP. NLBO has potential application as a nonlinear optical material [8].

As there are no theoretical calculations of the linear and nonlinear optical properties for NLBO crystal, we report such calculations in this paper and try to find the physical origin of the observed anisotropy. Therefore, research combining theoretical calculations and experimental measurements is necessary for understanding the electronic and optical properties and checking the validity of theoretical calculation. Our work will highlight the accuracy of the full potential calculation in comparison with our measurement.

Our aim in this paper is to understand the origin of the high $\chi^{(2)}(\omega)$ and the degree of birefringence in these materials.

2. Computational method

$Na_3La_9O_3(BO_3)_8$, ternary oxyborate nonlinear single crystals, crystallize in space group $P\bar{6}2m$ with a unit cell of dimensions $a = 8.9033$ Å and $c = 8.7131$ Å for $Z = 1$ [1, 2]. Its basic structure is composed of BO_3 planar triangles, LaO_9 polyhedra, LaO_8 polyhedra, and NaO_6 polyhedra.

The calculations reported in this work were carried out by means of the full potential linearized augmented plane wave (FP-LAPW) method using the WIEN2K computer package [11]. In this approach the space is divided into an interstitial region (IR) and non-overlapping muffin-tin (MT) spheres centered at the atomic sites. In the IR region, the basis set consists of plane waves. Inside the MT spheres, the basis set is described by radial solutions of the one particle Schrödinger equation (at fixed energy) and their energy derivatives multiplied by spherical harmonics. The exchange–correlation (XC) effects for the structural properties are treated by the local density approximation (LDA) [12]. The conventional band gap in LDA is not easy to fix by methods other than either very primitive (scissor) or quite sophisticated (GW) ones, for localized states like La f. So we can say that the position of La f band as it comes from LDA calculations is very far off.

In order to achieve energy eigenvalue convergence, the wavefunctions in the interstitial region were expanded in plane waves with a cutoff $K_{\max} = 9/R_{\mathrm{MT}}$, where R_{MT} denotes the smallest atomic sphere radius and $K_{\max}$ gives the magnitude of the largest K vector in the plane wave expansion. The R_{MT} are taken to be 2.0, 1.4, 1.2 and 1.3 atomic units (au) for La, Na, B and O respectively. The valence wavefunctions inside the spheres are expanded up to $l_{\max} = 10$, while the charge density was Fourier expanded up to $G_{\max} = 14$. The self-consistent calculations are considered to be converged when the total energy of the system is stable within 10^{-4} Ryd. The integrals over the Brillouin zone are performed up to 250 $\boldsymbol{k}$-points in the irreducible Brillouin zone (IBZ).

The BZ integrations are carried out using the tetrahedron numerical method [13, 14]. The frequency dependent linear optical properties are calculated using 500 $\boldsymbol{k}$-points and the nonlinear optical properties using 1500 $\vec{k}$-points in the IBZ. Both the plane wave cutoff and the number of $\boldsymbol{k}$-points were varied to ensure total energy convergence.

3. Several experimental parameters of the $Na_3La_9O_3(BO_3)_8$ single crystals

The investigated $Na_3La_9O_3(BO_3)_8$ single crystals have been synthesized by spontaneous crystallization on a iridium cylinder put in melts consisting of binary oxides. The cooling rate was equal to about 1.6 K min^{-1}. Thermostabilization was equal to about 0.01 K. The mixture for the melt consisted of La_2O_3, sodium carbonate and borate acids. The content of sodium oxide was varied within 34.8–39.6% and La_2O_3 oxide varied within 28–31.6%. The solidification temperature was varied within 1107–1156 °C depending on sodium oxide. The obtained crystals had average sizes about $2 \times 2 \times 3$ mm^3.

In figure 1(a) we present polarized spectra of the investigated crystals for light polarization parallel to z and x. Their features show only a light spectral shift. One can see a slight anisotropy of the values of the absorption edge. The shape of the absorption may indicate several contributions of the defect trapping levels. Following the extrapolation procedure, the energy gap for the z direction is equal to about 5.18 eV and for the x direction 5.09 eV.

Simultaneously we have made measurements of the birefringence (figure 1(b)) for the XZ-plane cuts of the crystals. The measurements were performed by the Senarmont method for the samples with thickness about 200–300 μm. As a light source, the light from the spectrophotometer SF4 with spectral resolution of about 1.5 nm was used. The precision of the birefringence determinations was about 3×10^{-4}. One can see that the value of the birefringence is about 0.065–0.007 up to 3.4 eV. With the following increase of the energy we have substantial enhancement of the birefringence, achieving a value of about 0.124 at an energy of about 5 eV.

Additional information about the anisotropy for the optical properties can be obtained from analysis of the imaginary part of the dielectric susceptibility (see figures 1(c) and (d)) on the spectral range of the inter-band transitions. For this reason we have used the polished plate of the samples cut in the XZ plane. The measurements were made on the

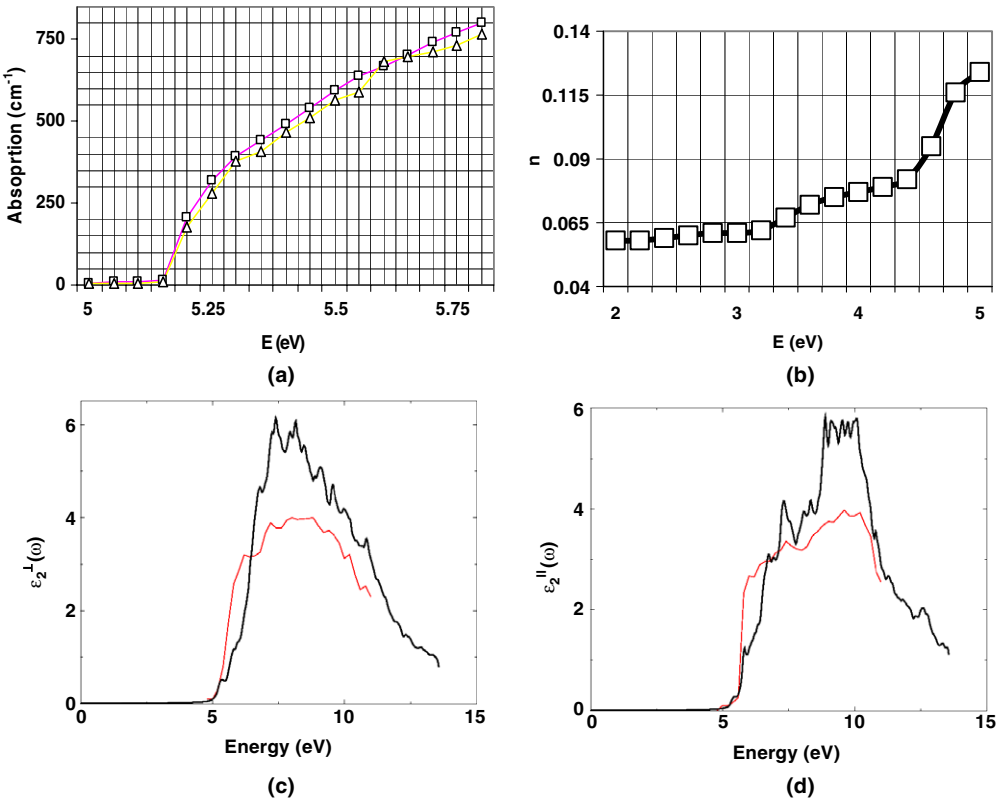

Figure 1. (a) Polarized absorption of the $Na_3La_9O_3(BO_3)_8$ single crystals for light polarization parallel to the z axis of the crystal (triangles) and x axis (squares). (b) Dispersion of the birefringence Δn_{xz}. (c) Calculated $\varepsilon_2^{\perp}(\omega)$ (dark curve) and measured (light curve). (d) Calculated $\varepsilon_2^{\parallel}(\omega)$ (dark curve) and measured (light curve).

Seya-Numioka based UV ellipsometer with spectral resolution about 6 nm. The light source was a He excited lamp. The grating monochromator allowed the measurements to be made in the reflected regime in a wide range of angles. The investigations have shown several anisotropies which may explain the observed anisotropy of the energy gap (see figure 1(a)) and of the birefringence (see figure 1(b)).

For investigations of the second order optical susceptibilities we have done an experiment using an optical parametrical oscillator (OPO) with the pumped 532 nm laser line. We have made the measurements for the two principal tensor components: d_{xxy} and d_{yyy}. In figure 2 we present the measured dependences for the two principal components of the second order optical susceptibilities for the investigated crystals. The dark line corresponding to d_{xxy} and d_{yyy} has a light line. One can see that the d_{xxy} tensor component has substantially larger value with respect to d_{yyy}.

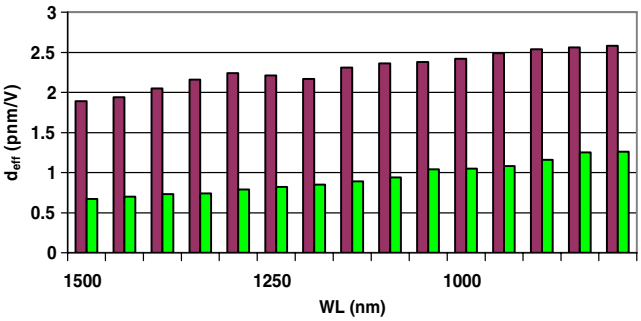

Figure 2. Spectral dependence of the second order optical susceptibilities for the two principal components: dark line, d_{xxy}; light line, d_{yyy}.

4. Results and discussion

4.1. First order optical susceptibilities and birefringence

Generally, optical properties of matter can be described by the mean of the transverse dielectric function $\varepsilon(\omega)$. There are two contributions to $\varepsilon(\omega)$, namely intra-band and inter-band transitions. The contribution from intra-band transitions is important only for metals. The inter-band transitions can further be split into direct and indirect transitions. Here we neglect the indirect inter-band transitions, which involve scattering of phonons and are expressed to give only a small contributions to $\varepsilon(\omega)$ [15]. To calculate the direct inter-band contributions to the imaginary part of the dielectric function $\varepsilon_2(\omega)$, one must sum up all possible transitions from the occupied to the unoccupied states. Taking the appropriate transition matrix elements into account, the imaginary part of the dielectric functions $\varepsilon_2(\omega)$ is given by [16]. The knowledge of both real and imaginary parts of the frequency dependent dielectric function allows the calculations of important optical functions such as the refractive index $n(\omega)$, reflectivity $R(\omega)$ and absorption coefficient $I(\omega)$; in this paper we will

concentrate on the calculation of the refractive index to explain the birefringence. The refractive index is given by the expression [17]

$$n(\omega) = \left[\frac{\varepsilon_1(\omega)}{2} + \frac{\sqrt{\varepsilon_1^2(\omega) + \varepsilon_2^2(\omega)}}{2} \right]^{1/2}.$$

In the calculations of the optical properties, a dense mesh of uniformly distributed $\boldsymbol{k}$-points is required. Hence, the Brillouin zone integration was performed with 286 $\boldsymbol{k}$-points in the irreducible part of the Brillouin zone. Broadening is taken to be 0.04 eV. Our optical properties are scissor corrected [18, 19] by 0.78 eV. This value is the difference between our calculated (4.44 eV) and measured (5.22 eV) energy gaps. This could be traced to the fact that LDA calculations usually underestimate the energy gaps. A very simple way to overcome this drawback is to use the scissor correction, which merely makes the calculated energy gap equal to the experimental gap.

Figures 1(c) and (d) display the variation of the imaginary (absorptive) part of the electronic dielectric function $\varepsilon_2(\omega)$. Our analysis of the $\varepsilon_2(\omega)$ curve show that the threshold energy (first critical point) of the dielectric function occurs at 5.2 eV. This point is the valence band minimum (VBM) and the conduction band maximum (CBM) splitting, which gives the threshold for direct optical transitions between the highest valence and the lowest conduction band. This is known as the fundamental absorption edge. Beyond these points, the curve increases rapidly. This is due to the fact that the number of points contributing towards $\varepsilon_2(\omega)$ increases abruptly. Generally, one can see a sufficiently good agreement with our experimental data (see figures 1(c) and (d)).

The principal peak in the spectra is situated at 8.0 eV for $\varepsilon_2^{\perp}(\omega)$ and 10.0 eV for $\varepsilon_2^{\parallel}(\omega)$. The imaginary part of the dielectric function $\varepsilon_2(\omega)$ is calculated from the electronic structure. More explicitly, $\varepsilon_2(\omega)$ is nothing but the one-electron approximation of the Fermi golden rule (sum over direct transitions times the delta function representing the conservation of energy). From the imaginary part of the dielectric function $\varepsilon_2^{\perp}(\omega)$ and $\varepsilon_2^{\parallel}(\omega)$ the real part $\varepsilon_1^{\perp}(\omega)$ and $\varepsilon_1^{\parallel}(\omega)$ is calculated by using Kramers–Kronig relations [20]. The static dielectric constant $\varepsilon_1(0)$ is given by the low energy limit of $\varepsilon_1(\omega)$. Note that we do not include phonon contributions to the dielectric screening, and $\varepsilon_1(0)$ corresponds to the static optical dielectric constant ε_∞. The calculated optical dielectric constant ε_∞ is 3.0 for $\varepsilon_1^{\perp}(0)$ and 2.8 for $\varepsilon_1^{\parallel}(0)$. The uniaxial anisotropy $[\delta\varepsilon = (\varepsilon_0^{11} - \varepsilon_0^{\perp})/\varepsilon_0^{\text{tot}}]$ is -0.068, indicating the strong anisotropy [21] of the dielectric function in the NLBO crystal.

Generally, the compound shows considerable anisotropy in the linear optical susceptibilities, which favors an important quantity in SHG and OPOs due to better fulfilling of phase matching conditions, determined by birefringence. The birefringence is the difference between the extraordinary and ordinary refraction indices, $\Delta n = n_e - n_0$, where in our case n_e is the index of refraction for an electric field oriented along the c-axis and n_0 is the index of refraction for an electric field perpendicular to the c-axis. The birefringence is important only in the non-absorbing region, which is below the energy gap. We have found that the birefringence $\Delta n(0)$ of the NLBO crystal is equal to 0.06, in qualitative agreement with our experimental data (see figure 1(b)). The static refractive index $n(0)$ is found to have the value 1.799 for $n^{\perp}(0)$ and 1.739 for $n^{\parallel}(0)$, which is in good agreement with those obtained by Yunge *et al* [10] at the wavelength of 1068 nm (table 1).

Table 1. Our calculated refractive index in comparison with previous calculated and measured ones.

Refractive index	This work	Previous calculations	Experimental
$n^{\perp}(0)$	1.799	1.8571[a]	1.8572[a]
$n^{\parallel}(0)$	1.739	1.771[a]	1.772[a]

[a] Reference [10].

4.2. Second order susceptibilities

The expressions of the complex second order nonlinear optical susceptibility tensor $\chi^{(2)}_{ijk}(-2\omega;\omega;\omega)$ have been presented in previous works [21, 22]. From the expressions we can obtain the three major contributions: the inter-band transitions $\chi^{ijk}_{\text{inter}}(-2\omega;\omega,\omega)$, the intra-band transitions $\chi^{ijk}_{\text{intra}}(-2\omega;\omega,\omega)$ and the modulation of inter-band terms by intra-band terms $\chi^{ijk}_{\text{mod}}(-2\omega;\omega,\omega)$. These are

$$\chi^{ijk}_{\text{inter}}(-2\omega;\omega,\omega) = \frac{e^3}{\hbar^2}\sum_{nml}\int \frac{\mathrm{d}\vec{k}}{4\pi^3}\frac{\vec{r}^{\,i}_{nm}\{\vec{r}^{\,j}_{ml}\vec{r}^{\,k}_{ln}\}}{(\omega_{ln}-\omega_{ml})} \times \left\{\frac{2f_{nm}}{(\omega_{mn}-2\omega)} + \frac{f_{ml}}{(\omega_{ml}-\omega)} + \frac{f_{ln}}{(\omega_{ln}-\omega)}\right\}$$

$$\chi^{ijk}_{\text{intra}}(-2\omega;\omega,\omega) = \frac{e^3}{\hbar^2}\int \frac{\mathrm{d}\vec{k}}{4\pi^3}\left[\sum_{nml}\omega_{nm}\vec{r}^{\,i}_{nm}\{\vec{r}^{\,j}_{ml}\vec{r}^{\,k}_{ln}\} \times \left\{\frac{f_{nl}}{\omega^2_{ln}\,(\omega_{ln}-\omega)} - \frac{f_{lm}}{\omega^2_{ml}\,(\omega_{ml}-\omega)}\right\} - 8\mathrm{i}\sum_{nm}\frac{f_{nm}\vec{r}^{\,i}_{nm}\left\{\Delta^j_{mn}\vec{r}^{\,k}_{nm}\right\}}{\omega^2_{mn}\,(\omega_{mn}-2\omega)} + 2\sum_{nml}\frac{f_{nm}\vec{r}^{\,i}_{nm}\{\vec{r}^{\,j}_{ml}\vec{r}^{\,k}_{ln}\}(\omega_{ml}-\omega_{ln})}{\omega^2_{mn}(\omega_{mn}-2\omega)}\right]$$

$$\chi^{ijk}_{\text{mod}}(-2\omega;\omega,\omega) = \frac{e^3}{2\hbar^2}\int \frac{\mathrm{d}\vec{k}}{4\pi^3}\left[\sum_{nml}\frac{f_{nm}}{\omega^2_{mn}(\omega_{mn}-\omega)} \times \{\omega_{nl}\vec{r}^{\,i}_{lm}\{\vec{r}^{\,j}_{mn}\vec{r}^{\,k}_{nl}\} - \omega_{lm}\vec{r}^{\,i}_{nl}\{\vec{r}^{\,j}_{lm}\vec{r}^{\,k}_{mn}\}\} - \mathrm{i}\sum_{nm}\frac{f_{nm}\vec{r}^{\,i}_{nm}\{\vec{r}^{\,j}_{mn}\Delta^k_{mn}\}}{\omega^2_{mn}(\omega_{mn}-\omega)}\right]$$

where $n \neq m \neq l$. Here n denotes the valence states, m the conduction states and l denotes all states $(l \neq m, n)$. There are two kinds of transitions which take place, one of them, vcc', involving one valence band (v) and two conduction bands (c and c'), and the second transition, $vv'c$, involving two valence bands (v and v') and one conduction band (c). The symbols are defined as $\Delta^i_{nm}(\vec{k}) = \vartheta^i_{nn}(\vec{k}) - \vartheta^i_{mm}(\vec{k})$ with $\vec{\vartheta}^i_{nm}$ being the i component of the electron velocity given as $\vartheta^i_{nm}(\vec{k}) = \mathrm{i}\omega_{nm}(\vec{k})r^i_{nm}(\vec{k})$ and $\{r^i_{nm}(\vec{k})r^j_{ml}(\vec{k})\} =$

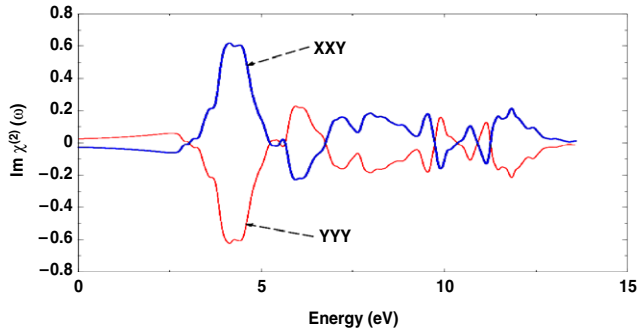

Figure 3. Calculated Im $\chi^{(2)}_{112}(\omega)$ (dark curve) and Im $\chi^{(2)}_{222}(\omega)$ (light curve). All Im $\chi^{(2)}(\omega)$ are expressed in units of 10^{-7} esu.

$\frac{1}{2}(r^i_{nm}(\vec{k})r^j_{ml}(\vec{k}) + r^j_{nm}(\vec{k})r^i_{ml}(\vec{k}))$. The position matrix elements between states n and m, $r^i_{nm}(\vec{k})$, are calculated from the momentum matrix element P^i_{nm} using the relation [23] $r^i_{nm}(\vec{k}) = \frac{P^i_{nm}(\vec{k})}{\mathrm{i}m\omega_{nm}(\vec{k})}$, with the energy difference between the states n and m given by $\hbar\omega_{nm} = \hbar(\omega_n - \omega_m)$. $f_{nm} = f_n - f_m$ is the difference of the Fermi distribution functions. i, j and k correspond to Cartesian indices.

It has been demonstrated by Aspnes [24] that only one virtual-electron transition (transition between one valence band state and two conduction band states) gives a significant contribution to the second order tensor. Hence we ignore the virtual-hole contribution (transition between two valence band states and one conduction band state) because it was found to be negative and more than an order of magnitude smaller than the virtual-electron contribution for these compounds. For simplicity we denote $\chi^{(2)}_{ijk}(-2\omega;\omega;\omega)$ by $\chi^{(2)}_{ijk}(\omega)$.

The investigated crystal belongs to the space group $P\bar{6}2m$, so there are only four independent components of the SHG tensor, namely, the $112 = 121 = 211 = -222$ components (1, 2, and 3 refer to the x, y, and z axes, respectively) [25]. These are $\chi^{(2)}_{222}(\omega)$, $\chi^{(2)}_{211}(\omega)$, $\chi^{(2)}_{112}(\omega)$, and $\chi^{(2)}_{121}(\omega)$. Where $\chi^{(2)}_{ijk}(\omega)$ is the complex second order nonlinear optical susceptibility tensor, $\chi^{(2)}_{ijk}(-2\omega;\omega;\omega)$ can be generally written as $\chi^{(2)}_{ijk}(\omega)$. The subscripts i, j, and k are Cartesian indices.

The calculated imaginary parts of the second order SHG susceptibilities $\chi^{(2)}_{112}(\omega)$ and $\chi^{(2)}_{222}(\omega)$ are shown in figure 3. We found that $\chi^{(2)}_{112}(\omega)$ is the dominant component, which shows the largest total Re $\chi^{(2)}_{ijk}(0)$ value (2.3 pm V^{-1}) compared to $\chi^{(2)}_{222}(\omega)$ (table 2). This is in accordance with our experimental data (see figure 2). This value shows very good agreement with the experimental data (2.0 pm V^{-1}) obtained by Zhang *et al* [8, 9]. A definite enhancement in the anisotropy on going from linear optical properties to nonlinear optical properties is evident (figure 3). It is well known that nonlinear optical susceptibilities are more sensitive to small changes in the band structure than the linear optical ones. Hence any anisotropy in the linear optical properties is enhanced more significantly in the nonlinear spectra.

In figure 4 we present the inter-band and intra-band contributions to the ω and 2ω resonances for the real and imaginary parts of $\chi^{(2)}_{112}(\omega)$. We note the opposite signs of the two contributions throughout the frequency range. We find that

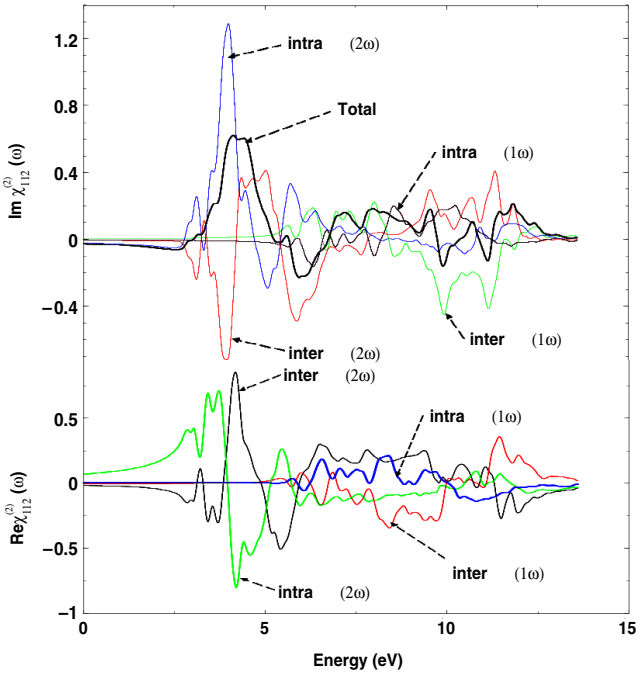

Figure 4. Calculated Im $\chi^{(2)}_{112}(\omega)$ and Re $\chi^{(2)}_{112}(\omega)$. All Im $\chi^{(2)}(\omega)$ are expressed in units of 10^{-7} esu.

Table 2. Calculated total and intra-/inter-band terms of the zero frequency of the real part of Re $\chi^{(2)}_{ijk}(\omega)$. The Re $\chi^{(2)}_{ijk}(0)$ total, inter, and intra are expressed in units of 10^{-7} esu. The total Re $\chi^{(2)}_{ijk}(0)$ pm V^{-1} is expressed in pm V^{-1}, in SI units.

Components	112	222
Re $\chi_{ijk}(0)$total	0.06	−0.06
Re $\chi_{ijk}(0)$inter	−0.02	0.02
Re $\chi_{ijk}(0)$intra	0.08	−0.08
Total	2.3	−2.3
Re $\chi_{ijk}(0)$ pm V^{-1}	2.0[a]	

[a] Reference [21] (experimental data).

the ω resonance is smaller than the 2ω resonance. As can be seen the total second order susceptibility determining SHG is zero below half the band gap. The 2ω terms start contributing at energies $\sim 1/2E_g$ and the ω terms for energy values above E_g. In the low energy regime ($\leqslant$5 eV) the SHG optical spectra is dominated by the 2ω contributions. Beyond 5.1 eV (values of the fundamental energy gaps) the major contribution comes from the ω term.

We have calculated the total complex susceptibility for $\chi^{(2)}_{112}(\omega)$ and $\chi^{(2)}_{222}(\omega)$. The real part of the two components is shown in figure 5. The zero-frequency limits of the two components for Re $\chi_{ijk}(0)$total, Re $\chi_{ijk}(0)$inter, Re $\chi_{ijk}(0)$intra, and total Re $\chi_{ijk}(0)$ pm V^{-1} are listed in table 2. The lack of experimental data prevents any conclusive comparison with experiment over a large energy range.

One could expect that the structures in Im $\chi^{(2)}_{ijk}(\omega)$ could be understood from the features of $\varepsilon_2(\omega)$. Unlike the linear optical spectra, the features in the SHG susceptibility are very difficult to identify from the band structure because of the presence of 2ω and ω terms. But we use the linear optical spectra to

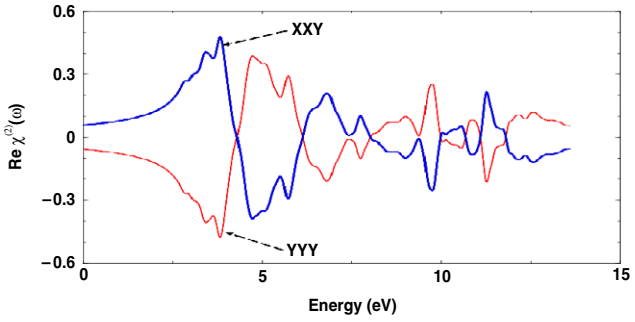

Figure 5. Calculated Re $\chi^{(2)}_{112}(\omega)$ (dark curve) and Re $\chi^{(2)}_{222}(\omega)$ (light curve). All Im $\chi^{(2)}(\omega)$ are expressed in units of 10^{-7} esu.

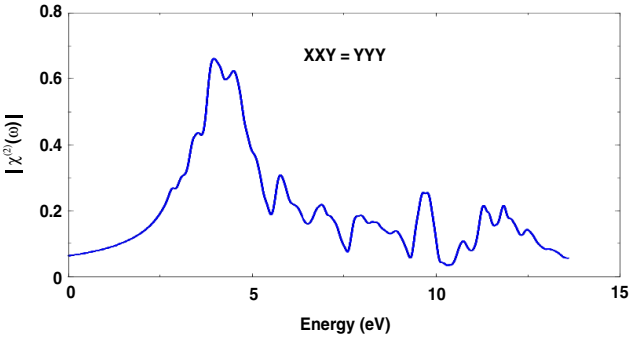

Figure 6. Calculated absolute values of $\chi^{(2)}_{112}(\omega)$; $\chi^{(2)}_{112}(\omega)$ is expressed in units of 10^{-7} esu.

identify the different resonances leading to various features in the SHG spectra. The first spectral band in Im $\chi^{(2)}_{123}(\omega)$ between 0.0 and 5.0 eV is mainly originated from the 2ω resonance and arises from the first structure in $\varepsilon_2(\omega)$. The second spectral band between 5.0 and 8.0 eV is associated with interference between the ω resonance and 2ω resonance and is associated with high structure in $\varepsilon_2(\omega)$. The last structure from 8.0–12.0 eV is mainly due to the ω resonance and is associated with the tail in $\varepsilon_2(\omega)$. Such features are typical for the borate crystals [26].

From an experimental viewpoint, one of the quantities of interest is the magnitude of SHG (proportional to the second order susceptibility). We present the absolute values of $\chi^{(2)}_{112}(\omega) = \chi^{(2)}_{222}(\omega)$ in figure 6. The first peak for these components is located at $2\omega = 4.6$ eV with the peak value of 0.7×10^{-7} esu.

5. Conclusions

We have performed experimental measurements and theoretical calculations of linear and nonlinear optical susceptibilities of novel $Na_3La_9O_3(BO_3)_8$, a ternary oxyborate nonlinear single crystal. Our first principle calculations of the linear and nonlinear optical susceptibilities for the NLBO single crystals within a framework of the FP-LAPW method are compared with our experimental measurements. Our calculations show that the edge of optical absorption for $\varepsilon_2^{\perp}(\omega)$ and $\varepsilon_2^{\parallel}(\omega)$ is located at 5.2 eV, in good agreement with our measurements. The anisotropy is in a good agreement with the theoretical calculations. The same is true for the birefringence. The imaginary and real parts of the second order SHG susceptibility $\chi^{(2)}_{222}(\omega)$ and $\chi^{(2)}_{112}(\omega)$ were evaluated. We note that any anisotropy in the linear optical susceptibilities will significantly enhance the nonlinear optical susceptibilities. Besides, we have established the 2ω inter- /intra-band contributions to the real and imaginary parts of $\chi^{(2)}_{ijk}(\omega)$, showing the opposite signs of the two contributions throughout the frequency range. This fact may be used in future for molecular engineering of the crystals in desirable directions. We found that our calculated and measured refractive indices are in good agreement with those obtained by Yunge *et al* [22] at the wavelength of 1068 nm (table 1). Our calculation shows that $\chi^{(2)}_{112}(\omega)$ is the dominant component, which shows the largest total Re $\chi^{(2)}_{ijk}(0)$ value (2.3 pm V^{-1}) compared to $\chi^{(2)}_{222}(\omega)$ (table 2). This value shows very good agreement with the experimental data (2.0 pm V^{-1}) obtained by Zhang *et al* [20, 21] and our measurements. A sufficiently good agreement of the calculated values of the optical parameters with the experimental ones was achieved.

Acknowledgments

This work was supported from the institutional research concept of the Institute of Physical Biology, UFB (No MSM6007665808), and the Institute of System Biology and Ecology, ASCR (No AVOZ60870520).

References

[1] Gravereau P *et al* 2002 *Solid State Sci.* **4** 993
[2] Wu Y C, Zhang G C, Fu P Z and Chen C T 2001 *Chinese Patent Application* No. 01134393.1 (Nov. 2, Publication no. CN052i010563)
[3] Becker P 1998 *Adv. Mater.* **10** 979
[4] Keszler D A 1999 *Curr. Opin. Solid State Mater. Sci.* **4** 155
[5] Sasaki T, Mori Y, Yoshimura M, Yap Y K and Kamimura T 2000 *Mater. Sci. Eng.* R **30** 1–54
[6] Chen G, Lin Z and Wang Z 2005 *Appl. Phys.* B **80** 1–25
[7] Aka G, Mougel F, Khan-Harari A, Vivien D, Benitez J M, Salin F, Pelenc D, Balembois F, Georges P, Brun A, Le Nain N and Jacquet M 2000 *J. Alloy Compounds* **303/304** 401
[8] Zhang G, Wu Y, Li Y, Chang F, Pan S, Fu P and Chen C 2005 *J. Cryst. Growth* **275** e1997–2001
[9] Zhang G, Wu Y, Fu P, Wang G, Pan S and Chen C 2001 *Chem. Lett.* **30** 456
[10] Li Y, Wu Y, Zhang G, Fu P and Bai X 2006 *J. Cryst. Growth* **292** 468–71
[11] Blaha P, Schwarz K, Madsen G K H, Kvasnicka D and Luitz J 2001 *WIEN2k, An Augmented Plane Wave Plus Local Orbitals Program for Calculating Crystal Properties* Vienna University of Technology
[12] Perdew J P and Zunger A 1981 *Phys. Rev.* B **23** 5048
[13] Jepsen O and Andersen O K 1971 *Solid State Commun.* **9** 1763
Lehmann G and Taut M 1972 *Phys. Status Solidi* b **54** 496
[14] Wilson J A and Yoffe A D 1969 *Adv. Phys.* **18** 193
[15] Smith N V 1862 *Phys. Rev.* B **3** 1971
[16] Hufner S, Claessen R, Reinert F, Straub Th, Strocov V N and Steiner P 1999 *J. Electron Spectrosc. Relat. Phenom.* **100** 191
Ahuja R, Auluck S, Johansson B and Kan M A 1994 *Phys. Rev.* B **50** 2128

[17] Wooten F 1972 *Optical Properties of Soilds* (New York: Academic)
[18] Levine B F 1973 *Phys. Rev.* B **7** 2600 and references therein
[19] Nastos F, Olejnik B, Schwarz K and Sipe J E 2005 *Phys. Rev.* B **72** 045223
[20] Tributsch H 1977 *Z. Naturf.* a **32A** 972
[21] Reshak A H 2005 *PhD Thesis* Indian Institute of Technology-Rookee, India
[22] Sharma S, Dewhurst J K and Ambrosch-Draxl C 2003 *Phys. Rev.* B **67** 165332
[23] Ambrosch-Draxl C and Sofo J O 2006 *Comput. Phys. Commun.* **175** 1
[24] Aspnes D E 1972 *Phys. Rev.* B **6** 4648
[25] Boyd W 1992 *Nonlinear optics* (Boston: Academic)
[26] Smok P, Kityk I V, Plucinski K J and Berdowski J 2002 *Phys. Rev.* B **65** 205103